S.C. Generalis[1], F.H. Busse[2]
[1]Aston University, Birmingham B4 7ET, U.K.
[2]University of Bayreuth, D-95440 Bayreuth, Germany

Abstract

Non-linear solutions and studies of their stability are presented for flows in a homogeneously heated fluid layer under the influence of a constant pressure gradient or when the mass flux across any lateral cross-section of the channel is required to vanish. The critical Grashof number is determined by a linear stability analysis of the basic state which depends only on the z-coordinate perpendicular to the boundary. Bifurcating longitudinal rolls as well as secondary solutions depending on the streamwise x-coordinate are investigated and their amplitudes are determined as functions of the supercritical Grashof number for various Prandtl numbers and angles of inclination of the layer. Solutions that emerge from a Hopf bifurcation assume the form of propagating waves and can thus be considered as steady flows relative to an appropriately moving frame of reference. The stability of these solutions with respect to three-dimensional disturbances is also analyzed in order to identify possible bifurcation points for evolving tertiary flows.

Nomenclature

g	acceleration of gravity	h	half channel width
q	volume strength of the heat source	χ	angle of inclination to the horizontal
$\boldsymbol{u}$	velocity	T	temperature
Π	pressure term	ν	kinematic viscosity
κ	thermal diffusivity	γ	coefficient of thermal expansion
Pr	Prandtl number ($Pr = \nu/\kappa$)	Gr	Grashof no ($Gr = (g\gamma q h^5)/(2\nu^2\kappa)$)

1 Introduction

This work is concerned with convection generated by uniformly distributed internal heat sources. The study here is motivated partially by previous work, but primarily by the fact that the present problem has many important environmental and industrial applications. Homogeneous heat sources may be caused, for example, by radioactivity in nuclear reactors. Homogeneous cooling at the boundaries may lead to the same mathematical problem as internal heating as long as the fluid properties are independent of the temperature (Krishnamurti, 1968ab). The problem of internal heat generation also arises in connection with convection in the Earth's mantle. Other applications include internal heating in fluids owing to the absorption of radiation such as the absorption of solar radiation in planetary atmospheres. In addition the present problem can be compared with Bénard convection, where motions are driven by temperature differences across the fluid layer and not by homogeneous heating. The present study focuses on the plane parallel shear flow with homogeneously distributed internal heat source with or without the imposition of the constraint that the mass flux across any lateral section of the channel flow is conserved. It is within this framework that internally heated parallel shear flow with a Poiseuille component is also examined. Direct comparisons of our numerical studies with published laboratory work of (Wilkie & Fisher, 1961) are not possible due to the various different conditions under which the experiments were performed.

2 Theory

We consider a viscous incompressible fluid bounded between two inclined parallel plates of infinite extent maintained at constant temperature $T = T_0$, where the cartesian coordinate system is positioned in the midplane of the fluid layer of width $2h$ with $\hat{\boldsymbol{i}}$,$\hat{\boldsymbol{j}}$ the unit vectors in the streamwise and spanwise (x, y) directions respectively. In the horizontal configuration the unit vector $\hat{\boldsymbol{k}}$ points in the direction opposite to gravity and coincides with the z axis of a Cartesian system of coordinates. For the non-dimensional description of our problem we apply the Boussinesq approximation and we use h, h^2/ν and $qh^2/2\kappa Gr$, as the units of length, time and temperature, respectively in order to obtain the following Navier-Stokes equations for the velocity vector $\boldsymbol{u}$ and for the deviation T of the temperature from the state of pure conduction

$$\frac{\partial \boldsymbol{u}}{\partial t} + (\boldsymbol{u}\cdot\nabla)\boldsymbol{u} = -\nabla\Pi + \Delta\boldsymbol{u} - \frac{\boldsymbol{g}}{g}T \tag{1}$$

$$\frac{\partial T}{\partial t} + (\boldsymbol{u}\cdot\nabla)T = \frac{1}{Pr}(\Delta T + 2Gr) \tag{2}$$

$$\nabla\cdot\boldsymbol{u} = 0 \tag{3}$$

$$\boldsymbol{u} = 0\ ,\ T = 0 \qquad at \quad z = \pm 1 \tag{4}$$

The boundary conditions are reflected by eqs.(4), where for convenience we have set $T_0 = 0$ for the fixed temperature of the boundaries, and no-slip condition at the boundaries for the velocity field. The Grashof number gives the strength of the internal heat source and terms that can be written as gradients have been combined into the expression $\nabla\Pi$. In our formulation the Rayleigh and Grashof numbers are related via the relation $Ra = Gr \times Pr$. The basic state for the vanishing mass flux case is described by (Gershuni & Zhukhovitskii, 1976, Generalis & Nagata 2003):

$$(\nabla\Pi_B)\cdot\boldsymbol{i} = -\tfrac{4}{5}Gr\frac{\boldsymbol{g}\cdot\boldsymbol{i}}{g} \tag{5}$$

$$\boldsymbol{u} = U_B(z)\hat{\boldsymbol{i}} = \tfrac{Gr}{60}\sin\chi(5z^4 - 6z^2 + 1)\hat{\boldsymbol{i}} \tag{6}$$

$$T = T_B = Gr(1 - z^2). \tag{7}$$

In previous work and when the Poiseuille component is considered, an alternative set of the Navier-Stokes equations has been derived, where the boundary conditions of eqs.(4) are applied and $R = -(1/2)d\Pi_B(x)/dx = U_{max}h/\nu$ is the Reynolds number that measures the strength of the applied pressure gradient in the streamwise direction (U_{max} is the maximum laminar velocity at midchannel for pure Poiseuille flow) (Ehrenstein & Koch 1991, Nagata & Generalis 2002):

$$\boldsymbol{u} = U_B(z)\hat{\boldsymbol{i}} = (\tfrac{Gr}{12}\sin\chi(z^4 - 6z^2 + 5) + R(1 - z^2))\hat{\boldsymbol{i}}\quad , \tag{8}$$

$$T = T_B = Gr(1 - z^2). \tag{9}$$

The basic velocity profile (for eq.(8) the condition $-Gr/2 \le R \le 0$, $Gr > 0$ must be satisfied) has two inflection points in $-1 \le z \le 1$[1] and so we can expect the steady basic state to be linearly unstable, although the Rayleigh instability criteria are applicable only to inviscid cases. The equations of the disturbances are presented and non-linear equilibrium states are examined for the zero mass flux (ZMF) case only in the present work. The ZMF case corresponds to the case where the remote ends of the channel are assumed to be closed, which in turn leads to the condition of vanishing mass flux through the layer cross-section.

In this work we present results in the case where temperature effects are ignored ($Pr = 0$), as well as when the competing thermal instability is taken into account ($Pr = 0.1, 7$). The

[1]For $R > 0$ these inflection points lie outside the channel width and for $R < -Gr/2$ there are no inflection points.

values of $Pr = 0, 0.1, 7$ are selected for the stability analysis and for the analysis of the evolving non-linear states in the special cases $\chi = 0°, 90°$. For this purpose we superimpose velocity and temperature disturbances $\hat{\boldsymbol{u}}$,$\hat{\theta}$ on the basic profiles and following (Busse, 1967) we separate the velocity and temperature disturbances into an average part (over the x, y coordinates) $\breve{U}(z,t)$, $\breve{T}(z,t)$ and a fluctuating part $\breve{\boldsymbol{u}}$,$\breve{\theta}$ (with a vanishing average over the x, y coordinates):

$$\hat{\boldsymbol{u}} = \breve{U}(z,t)\boldsymbol{i} + \breve{\boldsymbol{u}} = \breve{U}(z,t)\boldsymbol{i} + \nabla \times \nabla \times \phi \boldsymbol{k} + \nabla \times \psi \boldsymbol{k}, \tag{10}$$

$$\hat{\theta} = \breve{T}(z,t) + \breve{\theta}, \tag{11}$$

where ϕ, ψ are the poloidal and toroidal parts of the velocity fluctuations respectively. For such a decomposition the incompressibility condition is satisfied automatically, and plays no further part in the calculations. By applying the operators $\boldsymbol{\delta} = \nabla \times (\nabla \times \boldsymbol{k}\cdot)$ and $\boldsymbol{\eta} = \nabla \times (\boldsymbol{k}\cdot)$ we obtain the following equations for the poloidal ϕ and toroidal ψ parts of the velocity fluctuations

$$\begin{aligned} \partial_t \nabla^2 \Delta_2 \phi = \nabla^4 \Delta_2 \phi - \hat{U}\partial_x \nabla^2 \Delta_2 \phi + (\partial_z^2 \hat{U})(\partial_x \Delta_2 \phi) \\ + \sin\chi \partial_{xz}^2 \theta - \cos\chi \Delta_2 \theta - \boldsymbol{k} \cdot \nabla \times \nabla \times (\breve{\boldsymbol{u}} \cdot \nabla \breve{\boldsymbol{u}}) \end{aligned} \tag{12}$$

$$\begin{aligned} \partial_t \Delta_2 \psi = \nabla^2 \Delta_2 \psi + (\partial_z \hat{U})(\partial_y \Delta_2 \phi) - \hat{U}\partial_x \Delta_2 \psi \\ + \sin\chi \partial_y \theta + \boldsymbol{k} \cdot \nabla \times (\breve{\boldsymbol{u}} \cdot \nabla \breve{\boldsymbol{u}}) \end{aligned} \tag{13}$$

while we can rewrite the temperature equation in the form

$$\partial_t \theta = -\hat{U}\partial_x \theta + (\Delta_2 \phi)\partial_z (T_B + \breve{T}) + \frac{1}{Pr}\nabla^2 \theta - (\breve{\boldsymbol{u}} \cdot \nabla)\theta, \tag{14}$$

where we have dropped the $\breve{}$ from the temperature fluctuations, $\Delta_2 \equiv \partial_{xx}^2 + \partial_{yy}^2$ is the planform Laplacian and $\hat{U}(z,t) = U_B(z) + \breve{U}(z,t)$. Details of the numerical method followed here have been reported in (Nagata & Generalis 2002, Generalis & Nagata 2003). It is worth noting that for an orientation of the fluid layer other than the horizontal the system of eqs.(12-14) are solved in a moving frame of reference to account for the phase velocity of the non-linear equilibrium state.

2.1 ZMF case: $R = 0$

2.1.1 $Pr = 0, \chi = 90°$

In this section we calculate the non-linear equilibrium solutions that develop at the Hopf bifurcation points of the neutral curves as predicted by the linear analysis (Gershuni & Zhukhovitskii, 1976) due to two-dimensional disturbances (Squire's Theorem). Finite amplitude secondary steady solutions of eqs(12-14) can be obtained by representing ϕ in terms of orthogonal functions that satisfy the boundary conditions (4):

$$\phi = \sum_{\substack{l=0 \\ (m,n)\neq(0,0)}}^{L} \sum_{m=-M}^{M} \sum_{n=-N}^{N} a_{lmn}(1-z^2)^2 T_l(z) \exp[im\alpha(x-ct) + in\beta y], \tag{15}$$

with similar expressions for ψ, θ. Here $T_l(z)$ is the l-th order Chebyschev polynomial. Two different cases have been considered here, those for $Pr = 0, 7$, $R = 0$ and for the vertical inclination of the fluid layer ($\chi = 90°$). We report in this work our findings for $Pr = 0$ only. Here we ignore eq.(13) and the spanwise direction in eq.(15),setting $n = 0$. We thus assume $\psi = \partial_y = 0$, but we retain eqs.(12) (poloidal part). Equations of the form (Nagata & Generalis 2002, Generalis & Nagata 2003)

$$A\boldsymbol{x} + B\boldsymbol{x}^T\boldsymbol{x} = 0, \tag{16}$$

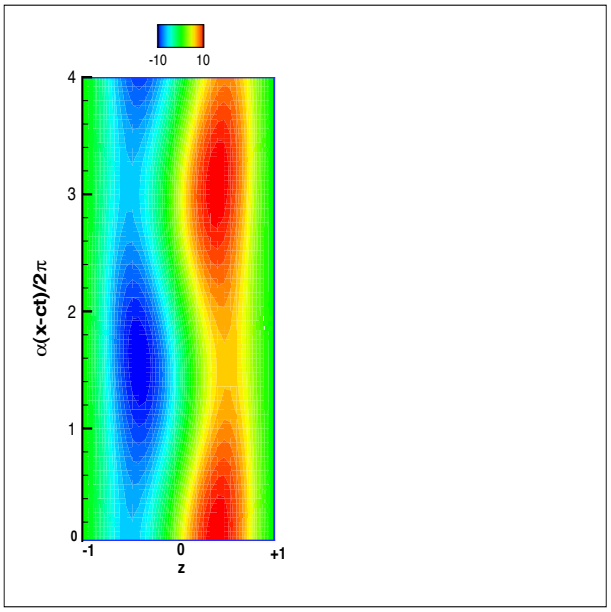

Figure 1: *The stream function of the total flow for the secondary traveling wave ($\beta = 0$). Here Gr=1850, α=2.07, Pr=0, $\chi = 90°$. The non-linear solution presented here corresponds to a traveling wave (TW) with phase velocity $c = 4.747$ indicating that the non-linear solution is a TW propagating upwards.*

where by x_i we denote collectively the unknown two-dimensional amplitudes that we evaluate at the collocation points $z_i = \cos((i+1)\pi/(N+2))$, $i = 0, \cdots, N$. The rank of A, B is $(L+1)(2M+1)$ and in our numerical work non-linear contributions to the phase velocity are evaluated explicitly by a transformation into the appropriately moving frame of reference.

In Figure 1 we present the structure of the secondary flow. From Figure 1 we observe that the flow is characterized by a sequence of transverse vortices (TR) aligned along the spanwise direction. The two dimensional equilibrium solutions consist of two sets of (counter rotating) vortices of positive and negative values. This creates a 'snake'-like wavy motion that oscillates between postive and negative values of the horizontal axis z. Similar meandering effects were observed in (Nagata & Generalis 2002, Generalis & Nagata 2003) and in the case of Poiseuille flow in (Ehrenstein & Koch 1991).

2.1.2 $Pr = 0.1, 7$, $\chi = 0°$, $R = 0$

In this section we present results for the horizontal fluid layer. For this case the basic mean flow and its nonlinear modifications vanish (for the ZMF case considered here $R = 0$). Moreover, because of the horizontal isotropy the eigenvalue problem is infinitely degenerate and an infinite number of convection patterns is possible in principle, as has been discussed in the analogous Bénard problem by (Schlüter, Lortz & Busse, 1965). Here we just focus on the convection patterns in the form of rolls, squares and hexagons, which are the only ones which provide periodic coverage of the horizontal plane. Our results for the non-linear equilibrium states for $Pr = 0.1$ are given in Figure 2 and for $Pr = 7$ are given in Figure 3 . Here

$$L_2^{\phi} = (\sum_{\substack{l=0 \\ (m,n)\neq(0,0)}}^{L} \sum_{m=-M}^{M} \sum_{n=-N}^{N} a_{lmn} a_{lmn}^*)^{1/2},$$

with similar expressions for L_2^{ψ},L_2^{θ}. The subcritical state corresponding to hexagonal convection cells with downward motion in the center (down HX) is the stable solution in contrast with the

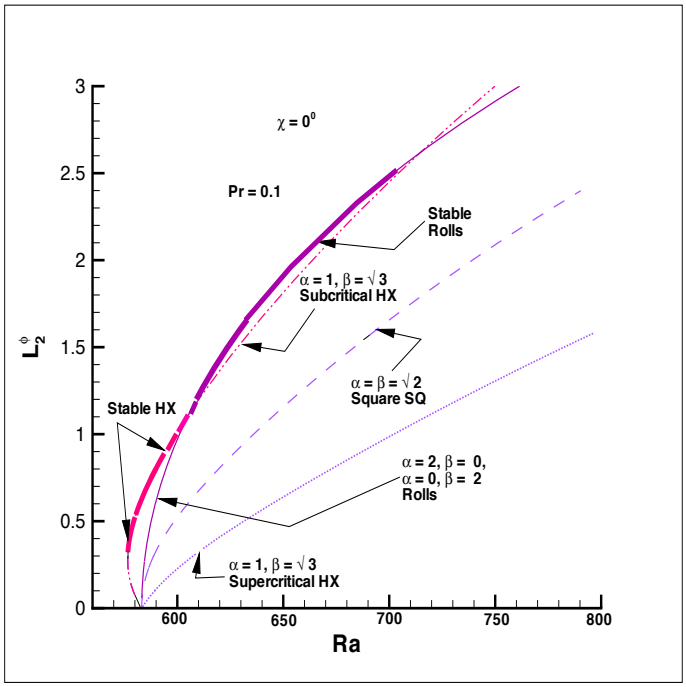

Figure 2: *L_2^ϕ-norms of the various nonlinear wave-like equilibrium solutions as functions of Ra for Pr=0.1. The bold parts on the L_2^ϕ-norm for rolls and the subcritical hexagon cells represent the range of Ra values for which those cells are stable.*

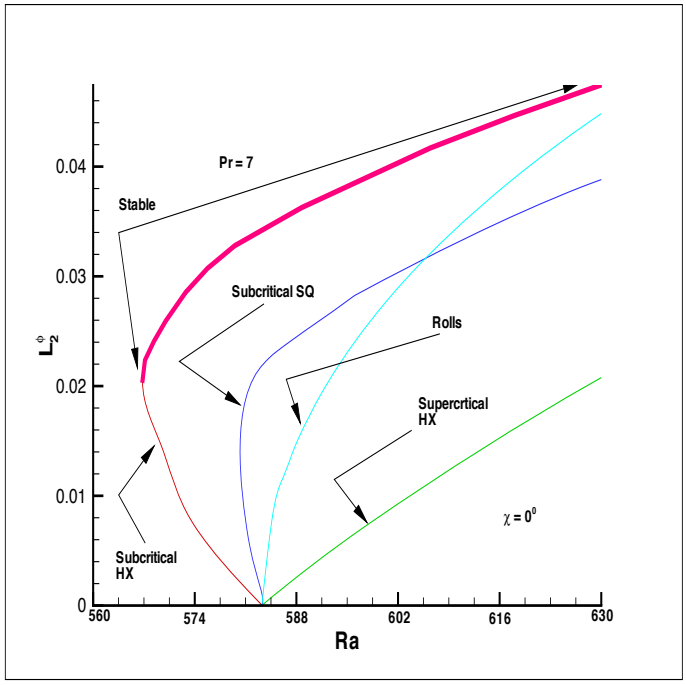

Figure 3: *L_2^ϕ-norms of the various nonlinear equilibrium solutions as functions of Ra for Pr=7. The bold part of the L_2^ϕ-norm for the subcritical hexagon cells represents the range of Ra values for which those cells are stable.*

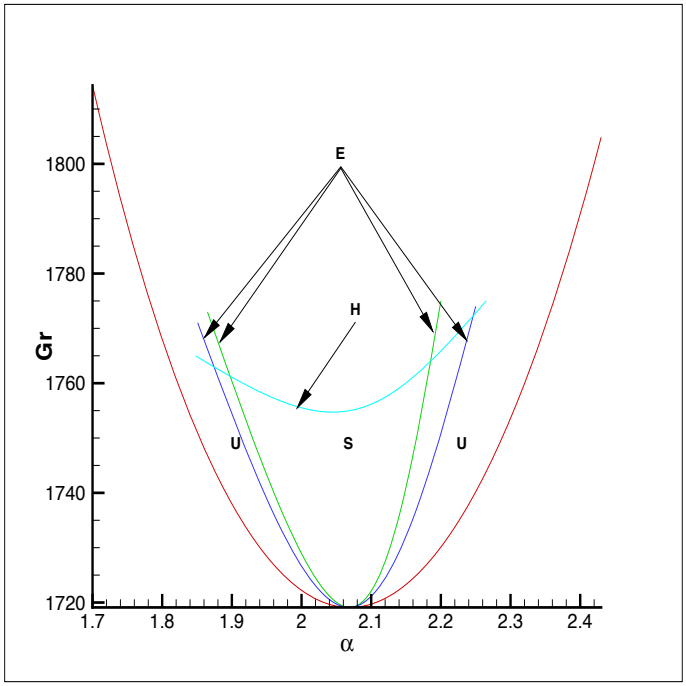

Figure 4: *Instability boundaries of secondary traveling waves for* $R = 0, Pr = 0, \chi = 90°$. *The stable region (S) of the secondary flow is bounded by the Eckhaus (E) and Hopf bifurcation (H) curves as indicated. For the outer Eckhaus boundary* $d = 0.001$, *while for the inner one* $d = 0.01$. *The outer boundary corresponds to the neutral curve of the instability of the basic flow descibed by eq.(6).*

supercritical state (up HX) that our numerical studies have shown to be unstable. The competition between rolls and hexagons for different values of the Prandtl number is of particular interest. In order to demonstrate this competition we have chosen to present results for a small value, $Pr = 0.1$, of the Prandtl number as well as a large one, $Pr = 7$. An unexpected result of our studies is the appearence of subcritical square patterns as depicted in Figure 3. Our studies have shown that the square patterns become subcritical for $Pr < O(1)$, while remaining supercritical for $Pr > O(1)$.

3 Stability of Secondary Flows and Discussion

The method for the numerical study of the linear stability of the secondary flow against three dimensional disturbances, in order to identify possible bifurcation points for the tertiary flow, is provided in detail in (Nagata & Generalis 2002, Generalis & Nagata 2003). In this section we have restricted ourselves to examining the stability of the flow for $Pr = 0, 0.1, 7$ and $R = 0$ and two orientations of the fluid layer; horizontal and vertical.

In Figure 4 we present the stability range of transverse traveling vortices for the case of the vertical orientation of the flow channel and for $Pr = 0$. It is bounded by the Eckhaus and Hopf bifurcation curves. For the Eckhaus curve, see Figure 4, which bounds the area of the stable transverse TWs towards larger and lower wavenumbers, the spanwise Floquet parameter assumes the value $b = 0$. A number of Eckhaus curves are plotted, depending on the value of the streamwise Floquet parameter d. In the case of the vertical orientation the secondary flow is stable in the region indicated. Maximum growth rates in the neighborhood of the Hopf bifurcation stability boundary are obtained for $d \approx \alpha, b = 0.2$. The fact that the H-stability boundary is characterized by $\sigma_{1i} = -27.72b$ indicates that the underlying (traveling) two-dimensional secondary flow is replaced by an obliquely propagating three-dimensional pattern.

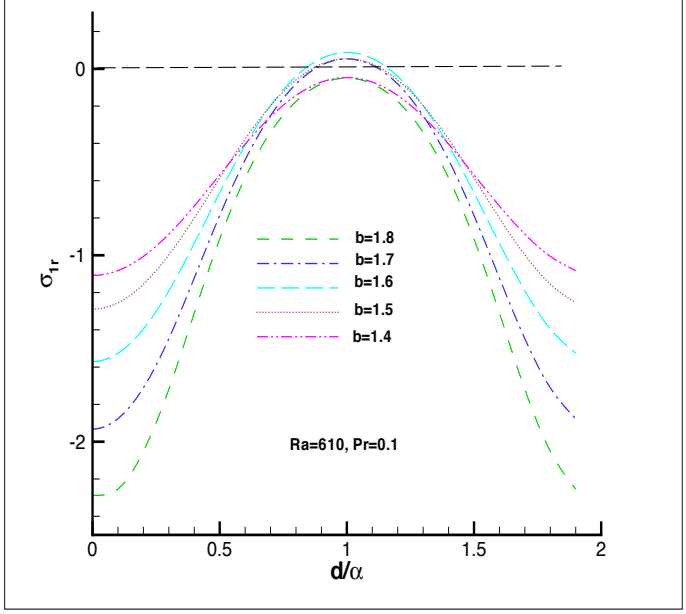

Figure 5: *Plots of the most dangerous eigenvalue as a function of the Floquet parameters for the rolls of the Figure 2 Here* $\alpha = 2.0, \beta = 0$, *or* $\alpha = 0, \beta = 2.0$, *Pr=0.1. The value* $Ra \approx 610$ *is where the amplitude of the* L_2^{ϕ} *of the rolls approximately exceeds that of the subcritical hexagons of Figure 2. For* $Ra > 610$ *the rolls become stable, while the hexagons become unstable. The values of the parameters* d, b, *for which maximum growth is observed, transform the wavenumbers of the roll type cell into those of a hexagon type cell.*

We next turn our attention to the horizontal configuration of the flow channel. Four forms of convection present themselves in this case. Two correspond to hexagonal cells [up or down] one to rolls and one to a square convective pattern. Our studies for the case $Pr = 0.1$ [see also figures 2 and 5] have shown that for this case the square pattern is always unstable and that the upper branch of the subcritical hexagonal pattern is exchanging stability with the supercritical rolls in the same scenario described in (Busse, 1967). When the Rayleigh number is increased the convection settles at the finite amplitude of the stable hexagon solution. In fact the subcritical hexagonal pattern becomes stable at the upper branch (from the turning point - see Figure 2). At approximately $Ra \approx 610$ the hexagonal pattern becomes unstable. A roll component of the hexagon grows and eventually the roll replaces the hexagon. The region of stable hexagons ends and the region of stable rolls starts at the point where $\sigma_{1r} = 0$ as the Ra value increases. In Figure 5 $\sigma_{1r} \approx 0$ for $d = 1$, $1.5 \leq b \leq 1.7$ and $Ra = 610$. Rolls prevail for values up to $Ra \approx 710$, where they become unstable. It appears therefore that the hexagonal convection becomes more efficient than the roll form of convection for Ra values close to the critical value, the latter type becoming more efficient as the Rayleigh number is increased provided the value of the Prandtl number is small. As Pr increases hexagonal convection becomes the predominant form of convection with the rolls being unstable, see Figure 3. As was shown in (Busse, 1967) the range of stable hexagonal cells vanishes as the asymmetry of material properties about the mid plane of the layer tends to zero. The selection of hexagons can therefore be attributed to the fact that homogeneous heating provides the asymmetry that removes the degeneracy within the framework of the Boussinesq approximation. Hexagons were also found theoretically and experimentally to represent a stable solution near the critical Rayleigh number by Krishnamurti (1968a,b) who used the property that homogeneous heating is equivalent to homogeneous cooling at the top and bottom boundaries. Apparently owing to a sign error in equ. (14) of Krishnamurti (1968a) the latter author had claimed that up-hexagons

are preferred in contrast to down-hexagons found in the present work and by other authors. See the discussion by Busse (1989). Hexagonal convection patterns were also observed in the recent experiments of (Tasaka, Kudoh, Takeda & Yanasigawa, 2005), where the infinite fluid layer was bounded by a conducting top and insulating bottom boundary. For the case where Pr exceeds a value of the order of unity and for the case of a fluid layer heated from below it has been shown that both types of hexagonal patterns can be stable for $Ra \approx 2 \times Ra_{crit}$ (Clever & Busse 1996). Reorientation of the hexgonal pattern and its transition to another hexagonal structure via the roll-route has very recently been observed experimentally in (Groh, Richter, Rehberg, Busse 2007). This has been achieved with the application of a magnetic field that is used to break the horizontal isotropy of the continuous system, the latter admitting the HX pattern as the common pattern for its instability evolution. This has also been evident in the calculations presented here but for higher values of the Prandtl number and also in the case where the angle of inclination of the channel flow is different from 0°. Details of the stability properties of the internally heated flow in the case of other values of the inclination angle and of Pr with or without the imposition of Poiseuille flow will be presented elsewhere.

4 References

Busse, F. H. 1989 Fundamentals of Thermal Convection, pp. 23-85 in *Mantle Convection*, W.R. Peltier, ed., Gordon and Breach Science Publishers.

Busse, F. H. 1967 The stability of finite amplitude cellular convection and its relation to an extremum principle, *J. Fluid Mech.*, **30**, 625-649.

Clever, R. M., & Busse, F.H. 1996 Hexagonal convection cells under conditions of vertical symmetry, *Phys. Rev. E*, **53**, R2037.

Ehrenstein, U. & Koch, W. 1991 Three-dimensional wavelike equilibrium states in plane Poiseuille flow, *J. Fluid Mech.*, **228**, 111-148.

Generalis, S. & Nagata, M. 2003 Transition in Homogeneously Heated Inclined Plane-Parallel Shear Flows, *ASME Journal of Heat Transfer*, **125**, 795-803, Transition in Plane-Parallel Shear Flows Heated Internally, 2004 *Comptes Rendus Mech.*, **332**, 9-16, Transition in Inclined Plane Parallel Shear Flows, 2006, *Japan Society of Fluid Mechanics*, **AM06-14-010**,186.

Gershuni, G. Z. & Zhukhovitskii, E. M. 1976 Convective stability of incompressible fluids, Keterpress Enterprises, Jerusalem.

Groh, C., Richter, R., Rehberg, I. & Busse, F.H. 2007 Reorientation of the Hexagonal pattern under broken symmetry: hexagon flip, *Phys. Rev. E*, **76**, 055301(R).

Krishnamurti, R. 1968a,b Finite amplitude convection with changing mean temperature, Parts 1. Theory; Part 2. An experimental test of the theory *J. Fluid Mech.*, **33**, 445-463.

Nagata, M. & Generalis, S. 2002 Transition in Convective Flows Heated Internally, *ASME Journal of Heat Transfer*, **124**, 635-642.

Schlüter, A., Lortz, D. & Busse F. H. 1965 On the stability of steady finite amplitude convection, *J. Fluid Mech.*, **23**, 129-144.

Tasaka Y., Kudoh Y., Takeda Y. & Yanasigawa T. 2005 Experimental investigation of natural convection induced by internal heat generation, *J. Phys., Conference Series* **14**, 168-179.

Wilkie, D. & Fisher, S. A. 1961 Natural convection in a liquid containing a distributed heat source, *International Heat Transfer Conference* **Paper 119**, University of Colorado, Boulder, 995-1002.